



Preparation and Characterization of Reduced Graphene Oxide /TiO₂ Blended Polyphenylene sulfone Antifouling Composite Membrane With Improved Photocatalytic Degradation Performance

Fengna Dai, Shangying Zhang, Qi Wang, Haiquan Chen, Chunhai Chen, Guangtao Qian* and Youhai Yu*

Center for Advanced Low-Dimension Materials, State Key Laboratory for Modification of Chemical Fibers and Polymer Materials, College of Material Science and Engineering, Donghua University, Shanghai, China

OPEN ACCESS

Edited by:

Leire Ruiz Rubio,
University of the Basque Country,
Spain

Reviewed by:

Vincenzo Vaiano,
University of Salerno, Italy
Hexing Li,
Shanghai Normal University, China

*Correspondence:

Guangtao Qian
qgt@dhu.edu.cn
Youhai Yu
yuyouhai@dhu.edu.cn

Specialty section:

This article was submitted to
Catalysis and Photocatalysis,
a section of the journal
Frontiers in Chemistry

Received: 05 August 2021

Accepted: 06 September 2021

Published: 19 October 2021

Citation:

Dai F, Zhang S, Wang Q, Chen H,
Chen C, Qian G and Yu Y (2021)
Preparation and Characterization of
Reduced Graphene Oxide /TiO₂
Blended Polyphenylene sulfone
Antifouling Composite Membrane With
Improved Photocatalytic
Degradation Performance.
Front. Chem. 9:753741.
doi: 10.3389/fchem.2021.753741

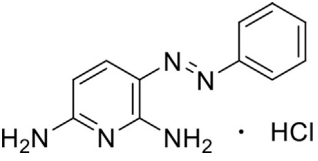
Nanosized titanium oxide (TiO₂)-based photocatalysts have exhibited great potential for the degradation of organic contaminants, while their weak absorption of visible light limits the photocatalytic efficiency. Herein, a novel reduced graphene oxide/TiO₂-polyphenylenesulfone (rGO/TiO₂-PPSU) hybrid ultrafiltration membrane has been successfully prepared via a non-solvent induced phase-separation method, in which the synergistic coupling between the rGO and TiO₂ could endowed the fabricated membranes with visible-light-driven efficient photocatalytically degradation of organic pollutants and outstanding photocatalytic and antifouling properties. Compared with the PPSU membranes prepared with Graphene oxide and TiO₂, respectively, the rGO/TiO₂-PPSU membrane demonstrated significant photodegradation towards phenazopyridine hydrochloride (PhP) solution under ultraviolet light (improved about 71 and 43%) and visible light (improved about 153 and 103%). The permeability and flux recovery rates of the membrane indicated that the high flux of the rGO/TiO₂-PPSU membrane can be greatly restored after fouling, due to the improved self-cleaning properties under visible light static irradiation. With the properties of high performance of photocatalytic degradation and good self-cleaning ability, the rGO/TiO₂-PPSU membrane would have great potential in water treatment.

Keywords: polyphenylenesulfone, reduced graphene oxide, titanium dioxide, photodegradation, self-cleaning

INTRODUCTION

The development of sewage and wastewater treatment is of utmost importance to address water crisis and obtain clean and safe drinking water (Brende, 2020). Ultrafiltration membrane technology has emerged as a cost-effective and sustainable application method in sewage and wastewater treatment in light of its excellent performance in separating particulates, organic pollutants and inorganic components in water. The ultrafiltration membranes are often based on organic polymers including polysulfone (PSF), poly(ether sulfone) (PES), polyphenylsulfone (PPSU), polyacrylonitrile (PAN)

TABLE 1 | Characteristics of phenazopyridine hydrochloride.

Structure	Formula	λ_{\max} (nm)	M _w (g/mol)	Solubility in Water (g/L, 25°C)
	C ₁₁ H ₁₂ N ₅ Cl	428	249.7	15.9

and polyvinylidene fluoride (PVDF) (Dharupaneedi et al., 2019). Among them, PPSU has attained great attention as an ideal membrane polymer in the field of membrane separation technology with its rigidity, good fluidity, good chemical corrosion resistance and high mechanical strength. However, due to its hydrophobicity, PPSU is prone to membrane fouling, which weakens the separation performance of the membrane, shortens the service life of the membrane and increases operation and maintenance cost of membrane (Golpour and Pakizeh, 2018; Dai et al., 2019; Kumar et al., 2021). In addition, the traditional membrane separation technology lacked the ability of removing all organic pollutants. Therefore, it is significant to explore a novel separation membrane system which can effectively address these issues.

Photocatalytic membrane reactor (PMR) based on the degradation of organic pollutants in water and wastewater through oxidation reactions was a prospective technology in water separation and purification driven by UV or visible light and facilitated the alleviation of membrane fouling without excessive waste of chemicals (Iglesias et al., 2016; Zhang et al., 2016; Kumari et al., 2020). Generally, the PMRs can be divided into two configurations: powder photocatalyst suspended in the reactor (SPMR) and photocatalyst fixed on the membrane (IPMR) (Espíndola et al., 2019). For SPMR, the recovery and post-treatment are principal challenges limiting its application. IPMR integrated both separation and photocatalytic properties, are easier to be recycled. The photocatalytic membranes (PMs) are the core to supported PMRs, in which the photocatalytic nanoparticles were attached to the membranes. The photocatalytic composite membranes can be prepared through different methods such as physical blending (Singh et al., 2020; Meng et al., 2021), self-assembly (Li et al., 2019), layer-by-layer assembly (Yan et al., 2019), chemical grafting or deposition (Ma et al., 2014; Pei et al., 2021). Among these, the physical blending is an effective and convenient manner because the membrane preparation process does not require additional operations during or after the phase transformation (Barzegar et al., 2020; Singh et al., 2020).

Numerous semiconductor photocatalysts have been reported, including TiO₂, ZnO, CdS, etc (Shen et al., 2020; Tran et al., 2020; Zangeneh et al., 2020; Yang et al., 2021). Among them, TiO₂ has garnered tremendous attention for its low-cost, nontoxicity, high catalytic activity, high chemical stability, acid and alkali resistance, photochemical corrosion resistance, non-pollution

and harmless to people (Mohd Hir et al., 2018; Zangeneh et al., 2019). When exposed to ultraviolet (UV) irradiation, TiO₂ can effectively decompose most organic compounds. This is because the band gap energy of TiO₂ is lower than the energy of ultraviolet radiation, which can excite titanium dioxide to produce photoelectrons (e⁻) and holes (h⁺). The e⁻ and h⁺ respectively react with O₂ and H₂O to form free radicals such as •O₂⁻ and •OH. The strong oxidizing radicals (•O₂⁻ and •OH) and h⁺ could directly participate in the decomposition of organic pollutants (Georg and James, 1995). Furthermore, the superhydrophilicity of TiO₂ will modulate surface morphology, improve permeability, and boost the self-cleaning and antifouling ability of membranes (Romay et al., 2020). However, UV light is an important factor to accelerate the aging of polymer membrane and shorted the service life of photocatalytic membranes. Hence, it is vital to develop PMs working in sunlight to realize water purification and reduce membrane aging during prolonged use.

Recently, it has been shown that the combination of graphene and its derivatives with TiO₂ is an effective way to reduce the electron hole recombination rate and improve its photocatalytic activity under visible light (Zhou et al., 2020; Hu F. et al., 2021; Xu et al., 2021). Graphene oxide (GO), obtained by chemically modified from graphene, is a novel material composed of sp² hybridized carbon atoms packing tightly into a monolayer two-dimensional honeycomb lattice structure. It has been widely applied in photocatalysis because of its large specific surface areas, high thermal conductivity, fast electron mobility and strong Young's modulus (Hu Y. et al., 2021). In rGO/TiO₂ nanocomposites, the network structure of rGO with large surface area and oxygen-containing functional groups are idea platforms for the tight-binding with TiO₂ to avoid the agglomeration of TiO₂ and enhance the photocatalytic effect of rGO/TiO₂. Moreover, the rGO nanosheets can accept the photoinduced electron conduction of TiO₂ and inhibit the electron hole recombination at the same time (Hunge et al., 2020; Chen et al., 2021).

The purpose of this study is to develop a novel kind of reusable photocatalytic rGO/TiO₂-PPSU hybrid UF membrane by physical blending and the non-solvent induced phase-separation method. The rGO/TiO₂ nanocomposites and the hybrid membranes were prepared and characterized. Using phenazopyridine hydrochloride (PhP) as a model containment, the photocatalytic degradation ability of the prepared membranes under both UV and visible irradiation was tested. The separation

TABLE 2 | The recipes of the membrane casting solutions.

Membranes	Mass ratio (wt%)			
	Nanomaterials	PPSU	PVP K30	NMP
PPSU	—	20	1	79
GO-PPSU	0.8	20	1	78.2
TiO ₂ -PPSU	0.8	20	1	78.2
rGO/TiO ₂ -PPSU	0.8	20	1	78.2

performance, as well as the antifouling and self-cleaning properties of the hybrid membranes were also evaluated.

MATERIALS AND METHODS

Materials

Polyphenylene sulfone (PPSU) was obtained from Shandong Horan Special Plastic Co., Ltd. (Weihai, China) 1-methyl-2-pyrrolidone (NMP) were obtained from Shanghai Lingfeng Chemical Co., Ltd. (Shanghai, China) Polyvinylpyrrolidone K30 (PVP K30, Mw = 44,000–54,000), Flake graphite (3,500 mesh), Potassium persulfate (K₂S₂O₈), sulfuric acid (H₂SO₄, 98%), Nitric acid (HNO₃, 68%), Phosphorus pentoxide (P₂O₅), Potassium permanganate (KMnO₄) and hydrogen peroxide were acquired from Sinopharm Chemical Reagent Co., Ltd. (Shanghai, China) Titanium dioxide (TiO₂, P25) was purchased from Degussa AG Co., Ltd. (Frankfurt, Germany) Phenazopyridine hydrochloride (PhP) was obtained from Adams Reagent Co., Ltd. (Shanghai, China) Characteristics of phenazopyridine hydrochloride were shown in **Table 1**. All reagents were applied without further purification.

Synthesis of GO and rGO/TiO₂ Nanocomposites

GO was synthesized first by natural graphite powder via a modified Hummer's method (Hummers and Offeman, 1958; Ding et al., 2019). In brief, 5 g graphite was uniformly dispersed in 300 ml of concentrated H₂SO₄ in a round-bottom flask, stirring for 5 min. After that, 4.2 g K₂S₂O₈ and 6.2 g P₂O₅ were slowly added, the mixture was heated and stirred at 80°C for 5 min. After filtration and drying, the product was transferred to a 200 ml beaker of concentrated H₂SO₄, and 15 g KMnO₄ was slowly added and vigorous agitation in an ice bath. The resulting mixture was treated with H₂O₂ until the gas ceased to be emitted. The resulting suspension was thoroughly washed, first three times with a diluted hydrochloric acid solution, then filtered with deionized water and centrifuged until the supernatant reached a pH of 7. The suspension was lyophilized to obtain pure GO powder.

The rGO/TiO₂ composites was prepared via a facile one-step hydrothermal method (Zhang et al., 2010). Basically, 22.5 mg GO was dispersed into a mixture of ethanol/water (2:1 v/v) and ultrasonicated for 60 min. After dispersing, 202.5 mg TiO₂ powder was added to agitate intensely for 5 h for a complete homogenization. Finally, a 30 ml mixture was transferred into a

100 ml Teflon-lined stainless autoclave and attained 120°C for 5 h. The obtained product was recovered through centrifuged with deionized water and ethanol and freeze-dried.

Preparation of rGO/TiO₂ Hybrid Ultrafiltration Membranes

The preparation of hybrid PPSU ultrafiltration membranes by solution casting and the non-solvent induced phase-separation method were based on previous study with a slight modification (Wang et al., 2021). Briefly, the casting solution, consisting of PPSU, the rGO/TiO₂ nanocomposites, PVP K30 (used as the porogen) and NMP (used as the solvent), were prepared under ultrasonication to obtain a homogeneous mixture, and then the mixture was further mechanical stirred at 300 rpm for 12 h. After bubble removal for 30 min, the casting solution was poured onto a clean glass plate with a scraper of 150 μm and immediately transferred to a water coagulation bath at 25°C until the membrane peeled off. Before testing, the resulting membranes were maintained in deionized water and replaced the water every 12 h. For comparison, GO-PPSU membranes, TiO₂-PPSU membranes and pristine PPSU membranes were prepared with the same procedure as mentioned above. The recipes of the membranes are shown in **Table 2**.

Characterization of GO and rGO/TiO₂ Nanocomposites

The morphology and microstructure of the GO and rGO/TiO₂ nanocomposites were characterized on the scanning electron microscopy (SEM; Regulus8230), transmission electron microscopy (TEM; JEM-2100) and high-resolution TEM (HRTEM; TecnaiG2F20). The crystalline structure of samples was observed by X-ray diffraction (XRD; RIGAKU, D/max-2550VB + /PC) equipped with Cu Kα radiation (18 kW, 10° ≤ 2θ ≤ 90°). The chemical composition of the membranes was characterized by using X-ray photoelectron spectroscopy (XPS, Thermo Scientific, Escalab 250Xi) provided with Al Kα source and Fourier transform infrared spectroscopy (FTIR; Bruker, VERTEX70) using KBr tableting method. The phase structure was observed by laser Raman spectrometer (Renishaw inVia-Reflex) using a 532 nm laser line in the wavelength range of 100–3,000 cm⁻¹ at room temperature.

Characterization of Membranes Membrane Characterization Techniques

The optical properties of hybrid membranes were investigated by using ultraviolet-visible diffuse reflection spectroscopy (UV-Vis DRS; PerkinElmer Instrument, 1901 Lambda 950). The top surface and cross section morphology of hybrid membranes were investigated by SEM after fracturing in liquid nitrogen and gold spraying. Energy dispersive X-ray (EDX) spectroscopy attached to SEM was employed to analyze the element composition. The surface hydrophilicity of hybrid membranes was detected by the water contact angle (WCA) using Drop Shape Analysis Data physics (OCA 20) at room temperature.

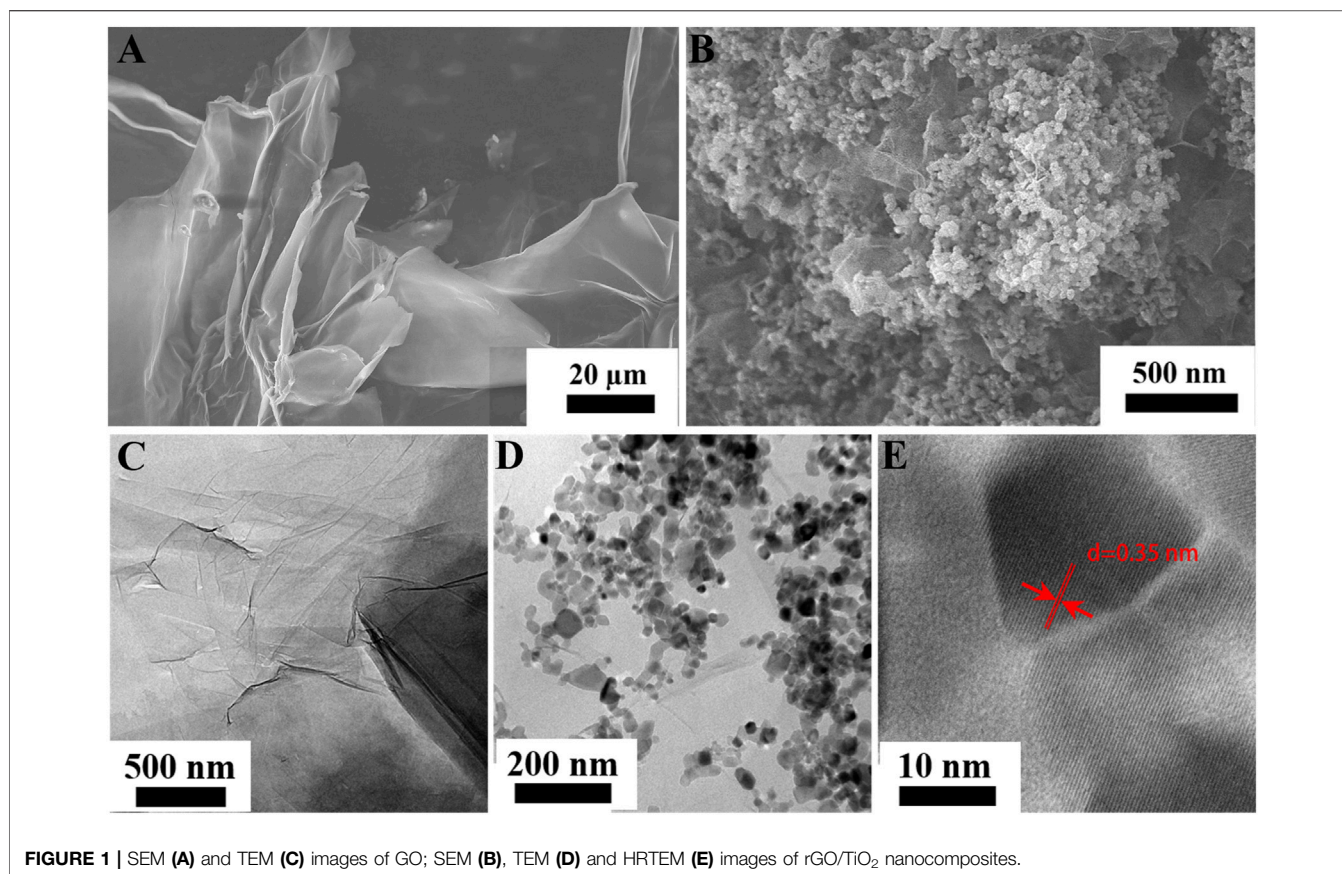


FIGURE 1 | SEM (A) and TEM (C) images of GO; SEM (B), TEM (D) and HRTEM (E) images of rGO/TiO₂ nanocomposites.

Permeation and Rejection of Membranes

Before measuring the pure water flux and PhP rejection, fabricated membranes were preloaded with DI water under the pressure of 0.2 MPa for 30 min. The permeate volume through the membrane was surveyed at 0.1 MPa, in which the feed solution was DI water and the PhP with a concentration of 15 mg/L respectively. The pure water flux (J_0) and PhP rejection (R) were calculated according to the following Eqs 1–2:

$$J_w = Q / (A \times \Delta T), \quad (1)$$

where Q is the volume of the penetrating fluid (L), A the effective area of the membrane (m²), and ΔT the filtration time (h).

$$R(\%) = (1 - C_p/C_f) \times 100\%, \quad (2)$$

where C_p (mg/L) and C_f (mg/L) are the PhP concentrations in the permeate and feed solution, respectively.

Photocatalytic Performance of Membranes

The photocatalytic performance of rGO/TiO₂-PPSU membranes and the three control membranes were measured by decomposing PhP under the condition of dark, UV light and visible light. The membranes were immersed into the reactor containing 150 mL of 15 mg/L PhP solution. Before photocatalytic experiment, the solution containing membranes was kept in darkness for 60 min to access adsorption equilibrium, and then the system was exposed to UV irradiation (250 W

mercury lamp) and visible irradiation (300 W Xenon lamp) for photocatalytic degradation. The concentrations of PhP were measured every 30 min using an ultraviolet spectrophotometer (PerkinElmer Precisely, Lambda950) at 428 nm. The PhP oxidation/mineralization tests were conducted by total organic carbon analyzer (TOC, Multi N/C 3100). The mineralization efficiency of PhP can be measured using Eq. 3:

$$TOC\ removal(\%) = [(TOC_0/TOC_t)/TOC_0] \times 100\%. \quad (3)$$

Anti-fouling Performance of Membranes

The flux recovery rate (FRR) is an important parameter employed to evaluate the antifouling performance of membrane. The pure water flux (J_0) of membranes were measured by the above steps. Then, the 15 mg/L PhP was served as feed solution to receive the flux of PhP solution (J_1) after 120 min. Afterwards, the fouled membrane surface was rinsed with DI water to remove loose pollutants, and the water flux of the rinsed membranes (J_2) was measured. Finally, the membranes were irradiated respectively under UV light and visible light for 30 min to remove contaminants on the membrane surface, and then test the water flux of the final clean membrane (J_3). The total fouling ratio (R_t), reversible fouling (R_r), irreversible fouling (R_{ir}) and FRR was calculated using Eqs 4–7:

$$FRR(\%) = (J_3/J_0) \times 100\%, \quad (4)$$

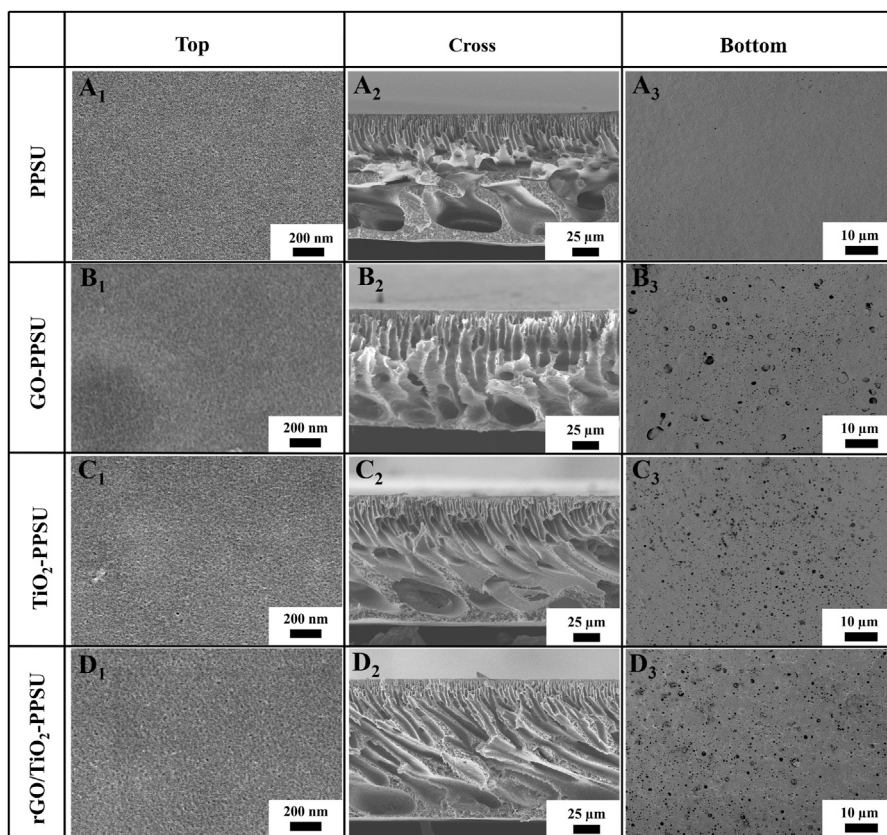


FIGURE 2 | SEM images of top, cross-sectional and bottom surface morphology: pristine PPSU (A₁, A₂, A₃), GO-PPSU (B₁, B₂, B₃), TiO₂-PPSU (C₁, C₂, C₃) and rGO/TiO₂-PPSU (D₁, D₂, D₃) membranes.

$$R_r (\%) = [(J_3 - J_1) / J_0] \times 100\%, \quad (5)$$

$$R_{ir} (\%) = [(J_0 - J_3) / J_0] \times 100\%, \quad (6)$$

$$R_t = R_r + R_{ir}. \quad (7)$$

RESULTS

Characterizations

Morphology

The microstructure of GO and rGO/TiO₂ nanocomposites was well examined by SEM and TEM are shown in **Figure 1**. In **Figures 1A,C**, the wrinkle and wormlike structures on GO surface indicate the successful preparation of GO. The SEM and TEM images of rGO/TiO₂ nanocomposites exhibited that TiO₂ were uniformly dispersed on GO in nanoscale dimension (**Figures 1B,D**). Dispersed TiO₂ nanoparticles on the surface of the GO sheets may prevent the stack of the GO sheets, while recombination between the GO sheets and the TiO₂ nanoparticles may weaken the aggregation of the TiO₂ nanoparticles (Liu et al., 2021). The corresponding HRTEM images (**Figure 1E**) revealed that the (101) lattice spacing of TiO₂ nanoparticles was estimated about 0.35 nm, which indicates that the TiO₂ nanoparticles on

GO sheets have fairly good crystallinity. The above SEM and TEM analysis showed that the TiO₂ nanoparticles were firmly attached on GO sheets, which was beneficial to the photodegradation activity of rGO/TiO₂ nanocomposites.

Figure 2 illustrated the top, bottom and cross section SEM views of pristine PPSU, GO-PPSU, TiO₂-PPSU, and rGO/TiO₂-PPSU membranes. The cross-section SEM images presented that the typical asymmetric porous structure consisting of the thin and dense skin layers, finger-like porous supporting layers, macroporous and sponge-like structure intermediate layers existed in all the fabricated membranes. With the supplementation of TiO₂, GO and the rGO/TiO₂ nanocomposites into the system, the finger-like porous of the hybrid membranes became wider, whereas larger-size pore and multiple pore numbers appeared on the top and bottom surface compared with the pristine PPSU membrane, which should be the result of faster exchange rate between solvents and non-solvents caused by increased thermodynamic instability. These meliorated typical structures played a critical role in enhancing the transmembrane transport capacity of water and improving the antifouling performance of membranes. The formation of the larger-sized pores was brought about for the reason that the

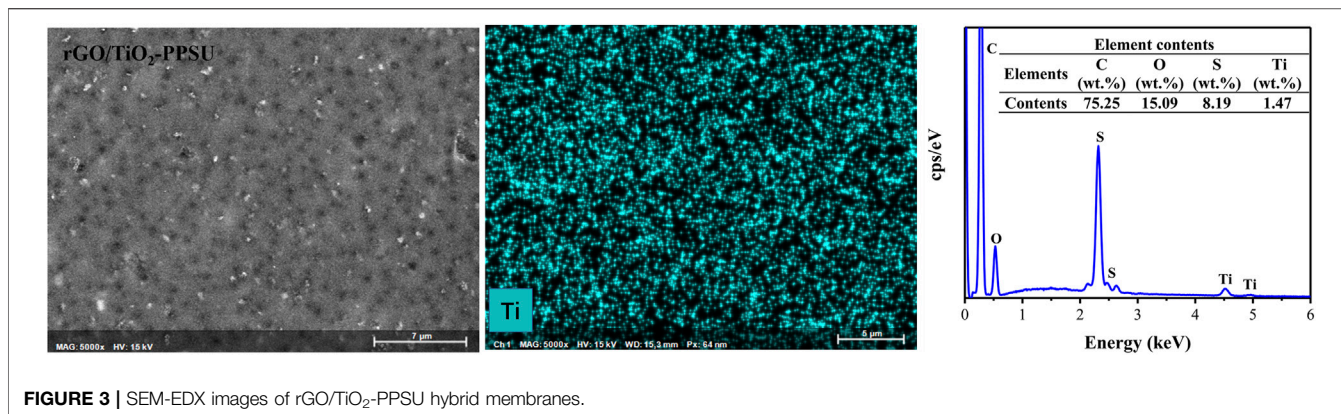


FIGURE 3 | SEM-EDX images of rGO/TiO₂-PPSU hybrid membranes.

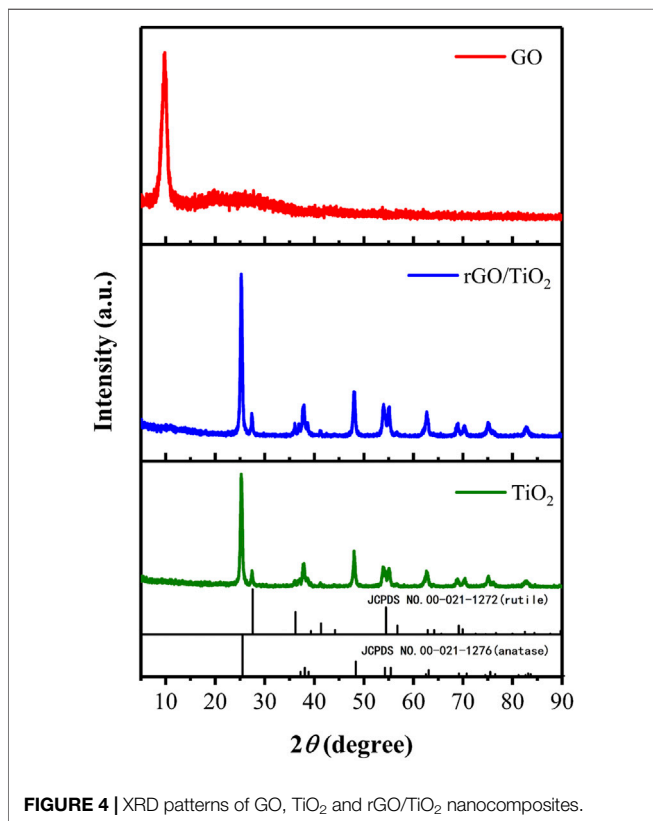


FIGURE 4 | XRD patterns of GO, TiO₂ and rGO/TiO₂ nanocomposites.

affinity between water and TiO₂, GO and the rGO/TiO₂ nanocomposite was higher than that between PPSU and water, which caused the permeation rate and exchange rate of solvent and non-solvent in the process of liquid-liquid phase transformation can be accelerated by mixing hydrophilic TiO₂, GO and the rGO/TiO₂ with PPSU, respectively (Xu et al., 2017). The SEM-EDX data of rGO/TiO₂-PPSU membranes reflected the ingredients of Ti elements (Figure 3), which indicated the existence of rGO/TiO₂ nanocomposites in the hybrid membranes.

Crystallinity

Figure 4 indicates the XRD patterns of GO, TiO₂ and rGO/TiO₂ nanocomposites. A sharp peak ($2\theta \approx 9.84^\circ$) in the XRD pattern of

GO sheets corresponded to the (001) inter-layer structure of GO sheets. The TiO₂ applied in this study consisted of a mixture of anatase type and rutile type, thus we infer that some characteristic peaks belonging to rutile TiO₂ (JCPDS cards No. 00-021-1276) at 2θ of 27.41° (110) and several characteristic peaks of anatase TiO₂ (JCPDS cards No. 00-021-1272) at 2θ of 25.29° (101), 37.87° (004), 48.14° (200), 54.01° (105), 55.05° (211), and 62.79° (204), 68.08° (116), 70.54° (220), 75.17° (215), 82.71° (224) in the XRD pattern of TiO₂ (Zhang et al., 2021). There are no obvious differences between the XRD pattern of TiO₂ and rGO/TiO₂, while the (001) diffraction peak of GO disappeared, which means that the insertion of TiO₂ may have disorganized the neat arrangement of GO sheets.

Chemical Composition

The FTIR spectrum of GO, TiO₂ and rGO/TiO₂ nanocomposites revealed in Figure 5A. For GO, the absorption peaks at 1,050, 1,252 and 1,393 cm⁻¹ owing to stretching mode of hydroxyl groups, epoxy C-O and O-H deformation, respectively. The characteristic peaks of C=O at 1,596 and 1,717 cm⁻¹ were assigned to the skeletal vibration of unoxidized graphitic domains and stretching carboxylic groups located on the edges of the graphene oxide sheets. The O-H stretching of GO appeared in the broad absorption band at 3,411 cm⁻¹. In the TiO₂ spectra, a wide absorption band about 620 cm⁻¹ corresponded to Ti-O-Ti stretching modes and a broad peak at 3,411 cm⁻¹ belong to the surface-adsorbed water and hydroxyl groups. With respect to rGO/TiO₂ nanocomposites, it can be seen that the majority of the GO peaks in the FTIR spectrum. The principal reason was that the formation of rGO during the hydrothermal synthesis process resulted in the disappearance of partial oxygen-containing functional groups on GO surface. In addition, the strong absorption band from 450 to 1,000 cm⁻¹ was remarkably expanded with the introduction of GO, confirming the presence of both the Ti-O-Ti and Ti-O-C bonds in the nanocomposites (Nguyen et al., 2020). As is shown in Figure 5B, the chemical structures of pristine PPSU and rGO/TiO₂-PPSU membranes were further identified by FTIR. The same absorption peak at 1,150 and 1,322 cm⁻¹ are corresponded to symmetric and asymmetric O=S=O stretches, and the peak at 1,235 cm⁻¹ can be assigned to the stretching C-O-C vibration. The peak

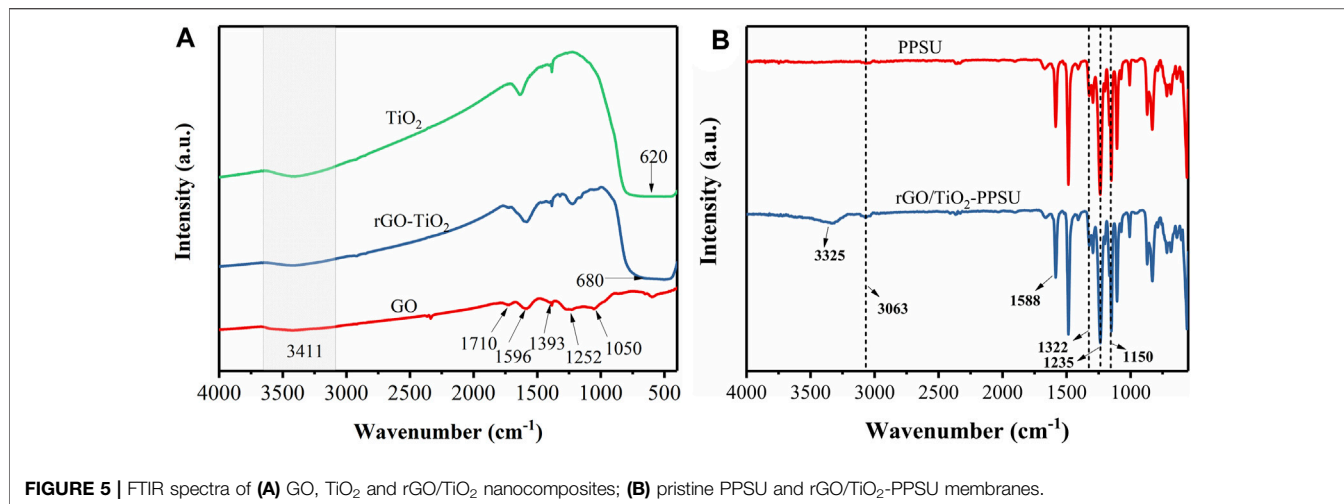


FIGURE 5 | FTIR spectra of (A) GO, TiO₂ and rGO/TiO₂ nanocomposites; (B) pristine PPSU and rGO/TiO₂-PPSU membranes.

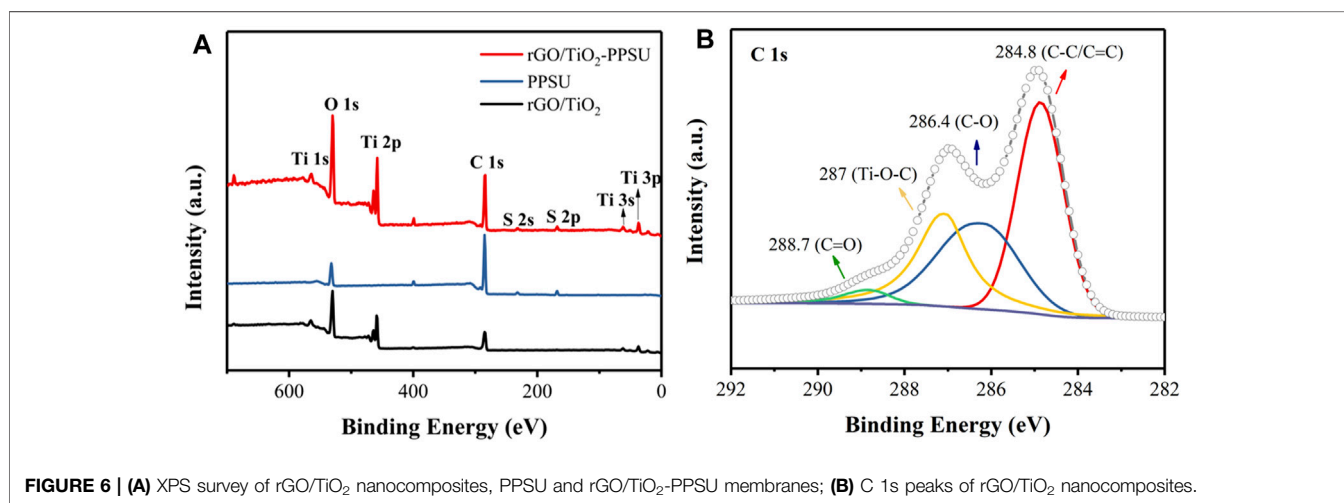


FIGURE 6 | (A) XPS survey of rGO/TiO₂ nanocomposites, PPSU and rGO/TiO₂-PPSU membranes; (B) C 1s peaks of rGO/TiO₂ nanocomposites.

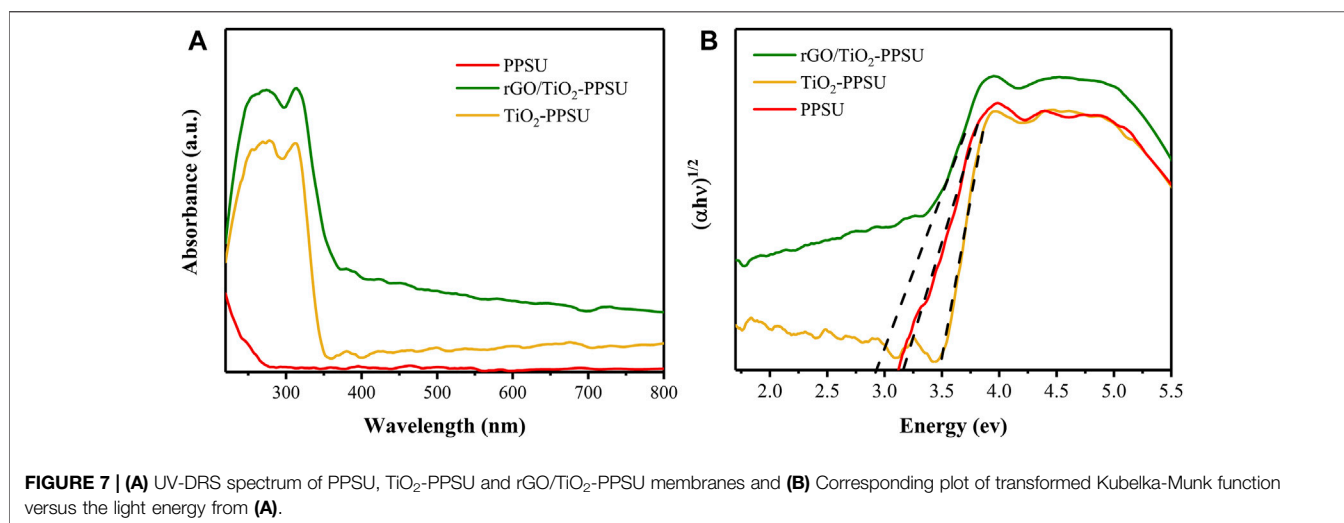
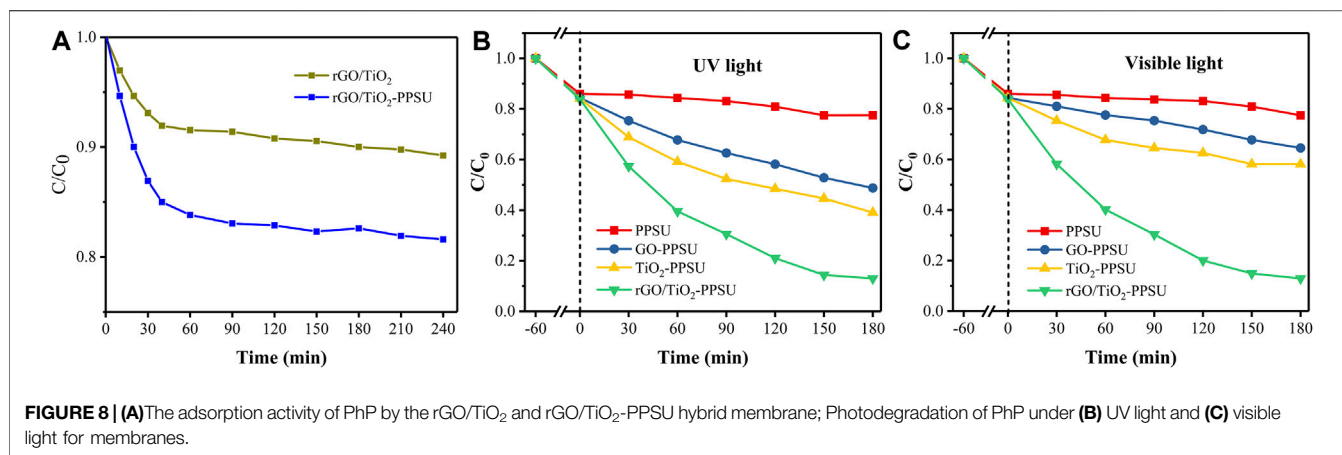


FIGURE 7 | (A) UV-DRS spectrum of PPSU, TiO₂-PPSU and rGO/TiO₂-PPSU membranes and (B) Corresponding plot of transformed Kubelka-Munk function versus the light energy from (A).



at 1,588 cm^{-1} can be attributed to the stretching C=O. The absorption peaks at 2,913 cm^{-1} and 3,058 cm^{-1} contributed to the aromatic and aliphatic stretching vibrations of $-\text{CH}_2$. Moreover, with the supplementary of the rGO/TiO₂ nanocomposites, a broad absorption peak at approximately 3,325 cm^{-1} due to the O-H stretching vibration in the rGO/TiO₂ nanocomposites emerged, which indicates the enhanced hydrophilicity of the hybrid membranes.

XPS spectra of rGO/TiO₂ nanocomposites, PPSU and rGO/TiO₂-PPSU membranes was showed in **Figure 6**. The peak at 458 eV in the XPS full survey (**Figure 6A**) and the peak at 287 eV in C 1s spectrum (**Figure 6B**) were major evidence for the existence of Ti and Ti-O-C bond, respectively. These results support the successful preparation of rGO/TiO₂ nanocomposites by hydrothermal synthesis. The XPS surveys in **Figure 6A** showed that the rGO/TiO₂-PPSU composite membrane consisted of the elements (C, O, S, and Ti) of both PPSU and rGO/TiO₂, which confirmed the successful immobilization of rGO/TiO₂ onto PPSU membranes.

Optical Properties

The UV-vis diffused reflectance spectra (UV-vis DRS) for the membrane of PPSU, TiO₂-PPSU and rGO/TiO₂-PPSU were shown in **Figure 7A**. The TiO₂-PPSU membrane performed a typical absorption band ca. 360 nm, while the rGO/TiO₂-PPSU membrane displayed a broad visible light absorption in the range of 400–800 nm because of the intercalation of GO, implying that the TiO₂-PPSU membrane was photocatalytically active under visible light (Xu et al., 2016). The corresponding band-gap values of the TiO₂-PPSU (3.48 eV) and rGO/TiO₂-PPSU (2.8 eV) membranes were extrapolated from the Kubelka-Munk function based on the reflectance values (**Figure 7B**), which was conducive to a more efficient use of visible light. Moreover, the pristine PPSU membrane has a short adsorption wavelength and a large band gap in connection with its high dielectric strength (14.6 kV/mm) and volume resistivity ($9 \times 10^{15} \Omega \cdot \text{cm}$). On the whole, the combination of rGO and TiO₂ altered its crystalline and electronic structures.

Photocatalytic Performance of Membranes

The adsorption-desorption process of the membrane in PhP solution was studied before the photocatalytic performance experiment. Compared with the rGO/TiO₂, rGO/TiO₂-PPSU membrane showed much higher adsorption capacity (**Figure 8A**). The result can be ascribed to twofold: firstly, although PPSU membranes are highly hydrophobic, the supplementary of rGO/TiO₂ caused a stronger adsorption of PhP solution on the membrane surface. Secondly, the unique porous structure of the membrane was also a vital parameter to promote adsorption. During the first 40 min of adsorption, the removal of PhP showed a rapid increase. After 40 min, the adsorption leveling off. Therefore, we selected 60 min of dark adsorption as the adsorption-desorption equilibrium point with the follow-up work.

The photocatalytic activity of rGO/TiO₂-PPSU membrane was estimated by monitoring the decomposition of PhP under UV and visible irradiation. The reference samples of pristine PPSU, GO-PPSU and TiO₂-PPSU membranes were studied under identical conditions, and the results were shown in **Figure 8**. As shown in **Figures 8B,C**, almost no photodegradation activity of PhP under UV and visible irradiation was observed for pristine PPSU membranes, suggesting that PPSU itself has practically no photocatalytic capability. By contrast, the hybrid membranes exhibited amplified photocatalytic activity doped with the TiO₂, GO and the rGO/TiO₂ nanomaterials under UV light. However, the GO-PPSU and TiO₂-PPSU membranes showed only limited decomposition of PhP relative to the rGO/TiO₂-PPSU membranes under visible irradiation. The main reason was that the wide band-gap energy of TiO₂ limits its photocatalytic activation only by UV irradiation. Notably, GO-PPSU membranes showed a fairly similar photocatalytic performance to TiO₂-PPSU membranes, suggesting that GO, as a semiconductor and photocatalyst itself, has a band-gap energy similar to TiO₂, which has also been reported by previous study (Gao et al., 2014). The rGO/TiO₂-PPSU membrane improved the removal rate of PhP, which was mainly related to the GO nanosheets supporting electron transfer and separation owing to their high charge mobility. The rGO/TiO₂-PPSU membrane showed higher photocatalytic activity both under UV and visible

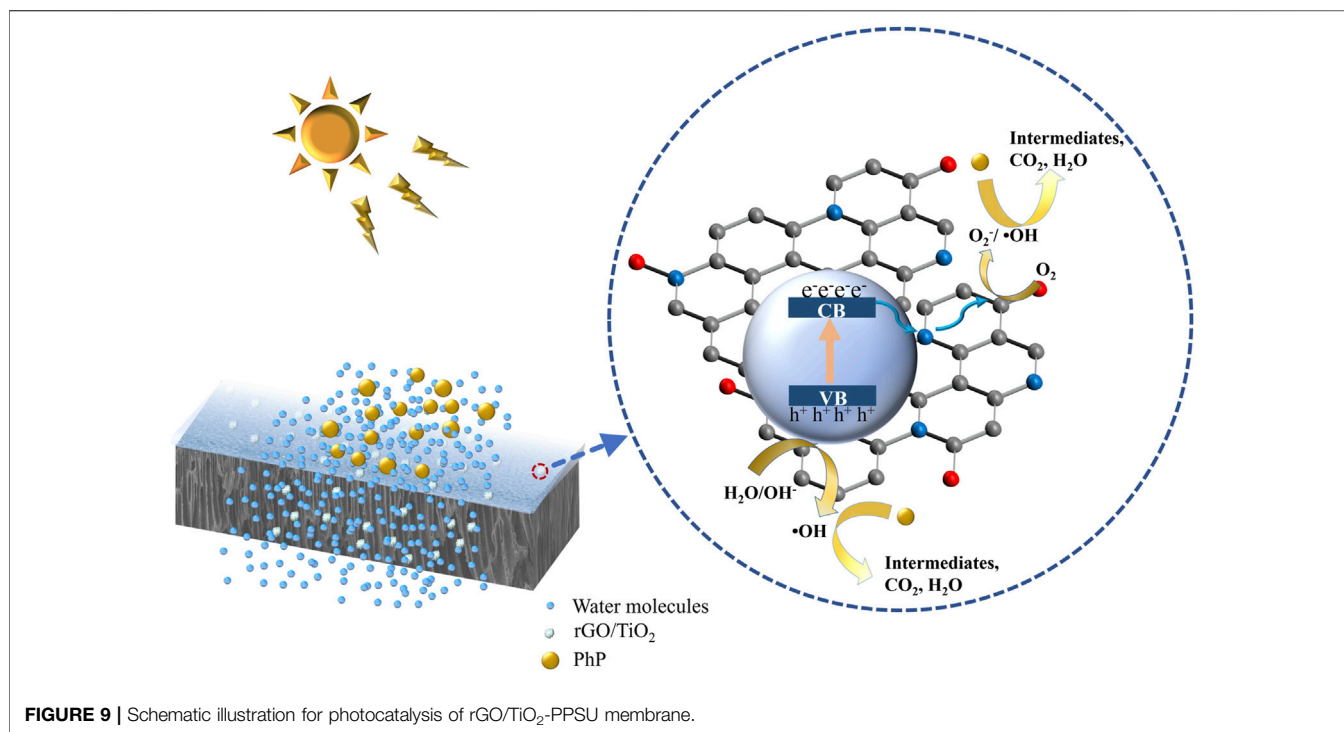


FIGURE 9 | Schematic illustration for photocatalysis of rGO/TiO₂-PPSU membrane.

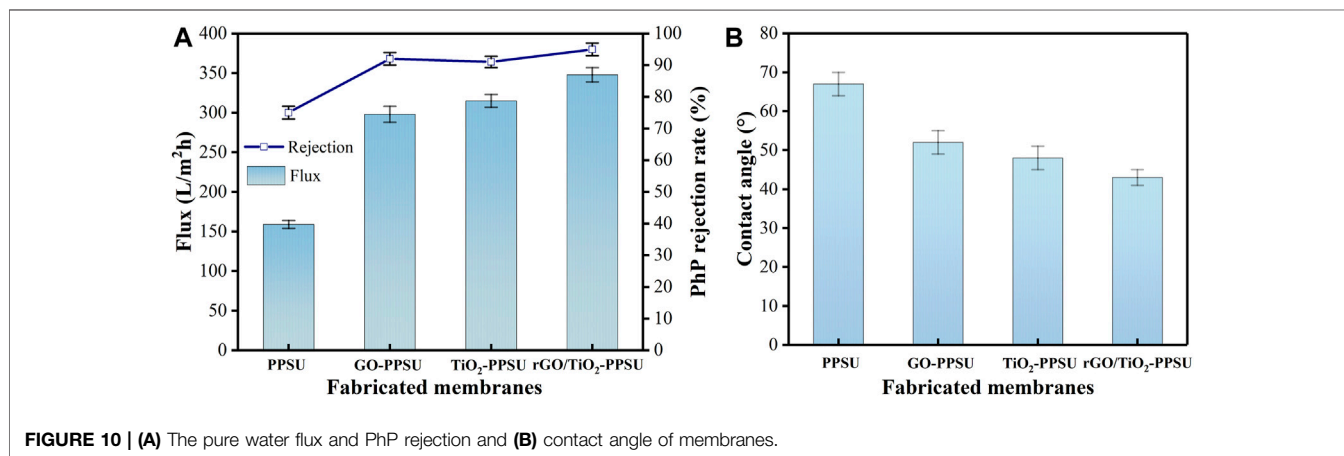
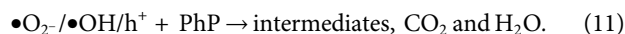
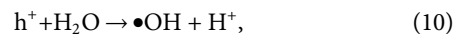
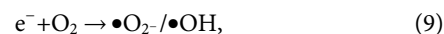
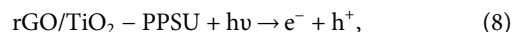


FIGURE 10 | (A) The pure water flux and PhP rejection and (B) contact angle of membranes.

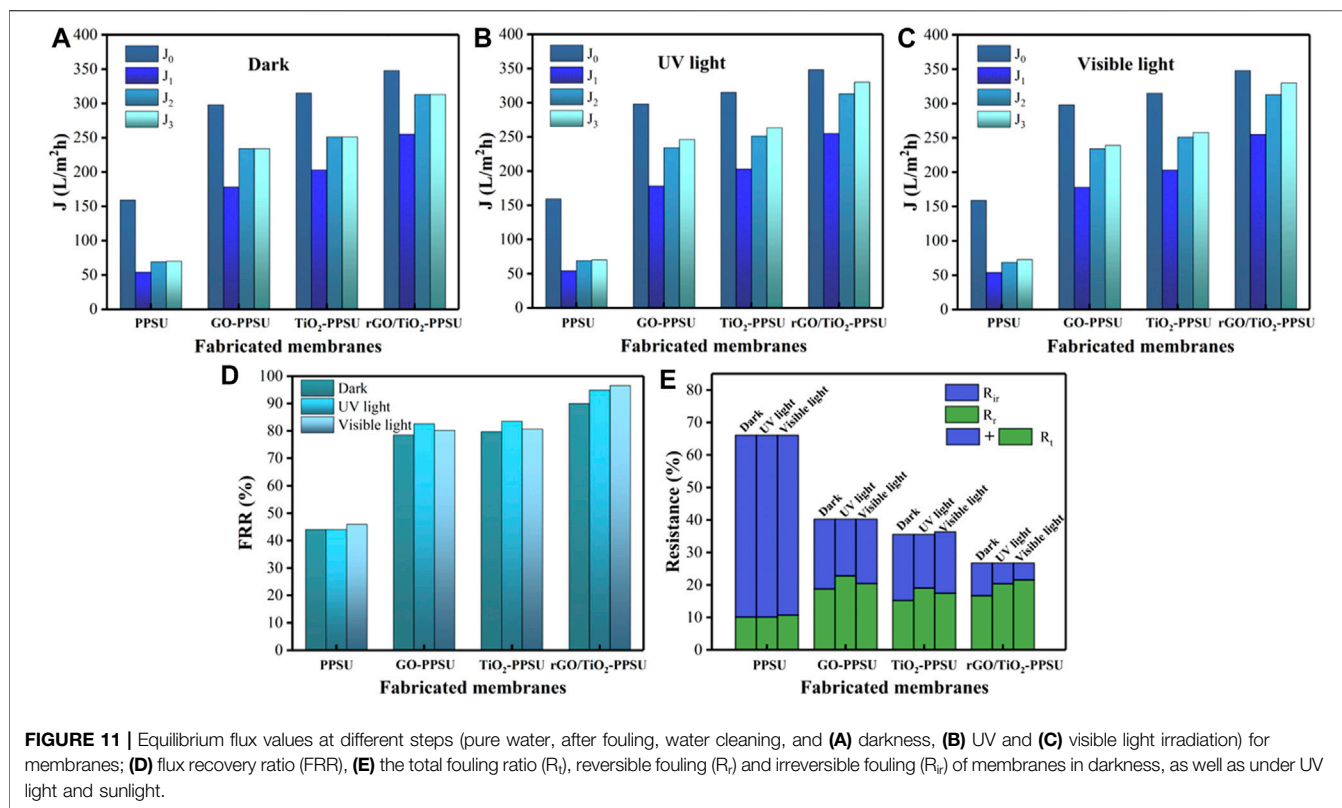
light for 180 min, and the PhP removal efficiency reached 87 and 87.1%, respectively. In brief, the combination of TiO₂ and rGO was beneficial to reducing the recombination effect of charge, narrowing the band-gap energy, expanding the light response range of the composite membranes to both UV and visible light range, and eventually improving the photocatalytic efficiency. The PhP photodegradation mechanism by the photocatalytic rGO/TiO₂-PPSU hybrid membrane could be illustrated in detail by **Figure 9** and **Eqs 8–11**. First, the hybrid membrane surface and pores were attracted with PhP molecules by the electrostatic adsorption. Then, the rGO/TiO₂ nanoparticles on the hybrid membrane were excited to produce photoelectrons (e⁻) and holes (h⁺) under UV/visible irradiation, which migrated to the surface of rGO/TiO₂. Finally, the e⁻ and h⁺ respectively

react with •O₂⁻ and H₂O to form free radicals such as •O₂⁻ and •OH. The strong oxidizing radicals (•O₂⁻ and •OH) and h⁺ could directly oxidize PhP into the intermediates, CO₂ and H₂O.



Permeability and Selectivity of Membranes

The permeability and selectivity of the rGO/TiO₂-PPSU membrane were measured by judging the pure water flux and PhP rejection. As shown in **Figure 10A**, all the hybrid membranes



doped with inorganic nanomaterials showed higher water permeation flux and higher separation efficiency related to the pure PPSU membranes, while the rejection of rPhP remained nearly constant of 94%. The pure water flux of rGO/TiO₂-PPSU membranes was 348.6 L/m²h, being 119% higher than that of PPSU membranes (159.3 L/m²h), 17% higher than that of GO-PPSU membranes (298.5 L/m²h) and 10% higher than that of TiO₂-PPSU membranes (315.9 L/m²h). The results mainly caused by the following two parameters: 1) The introduction of the membrane matrix with GO, TiO₂ and GO/TiO₂ nanomaterials with hydrophilic groups would endow the membrane excellent hydrophilicity, which was conducive to transport the water molecules across membranes (Abdel-Karim et al., 2021). As the results of contact angle shown in **Figure 10B**, the trend of improvement in contact angle was virtually consistent with the improvement of water permeability. 2) The appearance of porous structure of all the hybrid membranes resulted from the quick exchange between non-solvent and solvent during the phase transformation process was also beneficial to the water permeability promotion (**Figure 2**).

Anti-fouling Performance and Reusability of the rGO/TiO₂-PPSU Composite UF Membranes

The antifouling and self-cleaning properties of all membranes were investigated using four-step filtration operations including before and after fouling by 15.0 mg/L PhP solution, after the cleaning by rinsing and the exposure in darkness, as well as under

UV light and visible light, as shown in **Figure 11**. Obviously, the PhP flux presented significant decline due to fouling compared with pure water flux. However, the downward trend of the flux of the hybrid membrane was slower than that of the pure membrane, which can be attributed to the repulsive force between the pollutant and the membrane surface due to the increased electronegativity, indicating the enhancement of antifouling performance. The membrane permeate flux showed a limited recovery after removing loosely bound PhP with a backwash by straightforward distilled water. In order to further remove the fouling firmly adhering to the membrane surface and obtain a greater degree of flux recovery, the membranes were revealed to UV and visible irradiation, while the membrane was placed under dark conditions as a control group. **Figure 11A** showed the flux of all membranes have barely increase significantly after treatments. Nevertheless, after UV irradiation, the flux of all the hybrid membranes played further increased (**Figure 11B**), while after visible light irradiation, the flux recovery of the GO-PPSU and TiO₂-PPSU membrane was limited (**Figure 11C**). Compared with GO-PPSU and TiO₂-PPSU membrane, as showed in **Figure 11D**, the rGO/TiO₂-PPSU membrane exhibited the superior flux recovery rate under UV and visible irradiation, which was similar to the photocatalytic degradation trend of PhP observed previously (**Figure 8**). The higher FRR, the better anti-fouling ability. In **Figure 12E**, the R_{ir} of PPSU membrane was 55.97, 55.89 and 55.35%, respectively; the R_t was 66.03, 65.95 and 66.04%, respectively. High values of R_{ir} and R_t mean more resistant fouling on the PPSU membrane surface, which cannot be

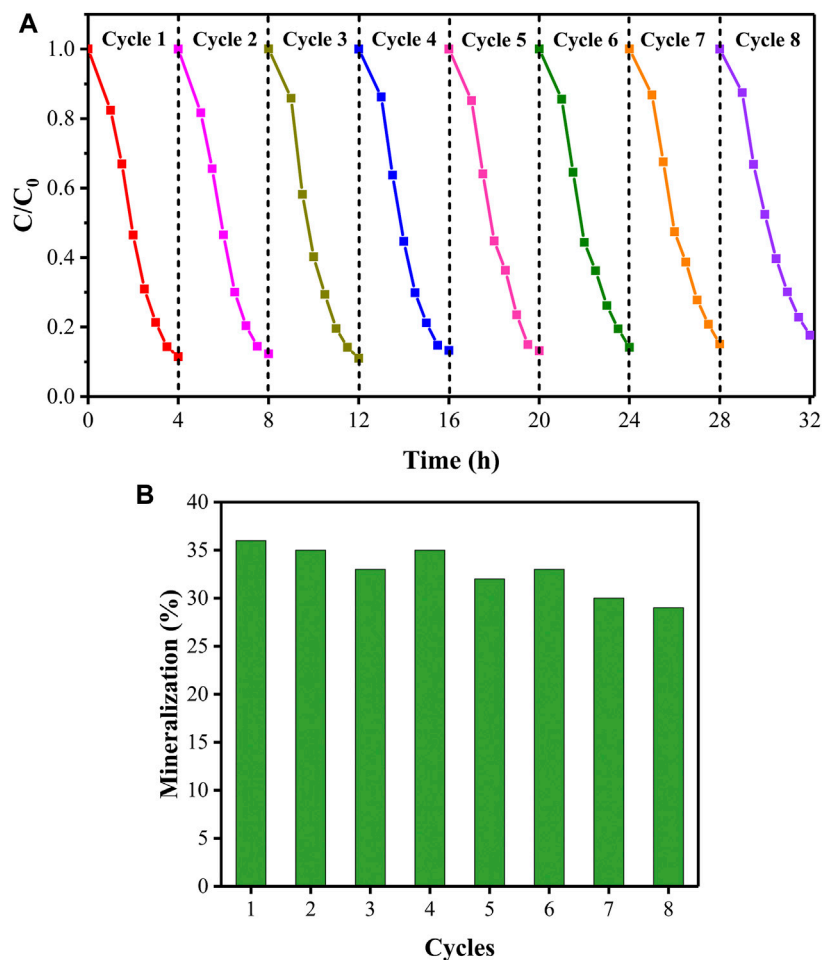


FIGURE 12 | The removal rate (A) and mineralization rate (B) of PhP in the process of recycling under visible light irradiation (initial PhP concentration of 15 mg/L, initial pH of 8).

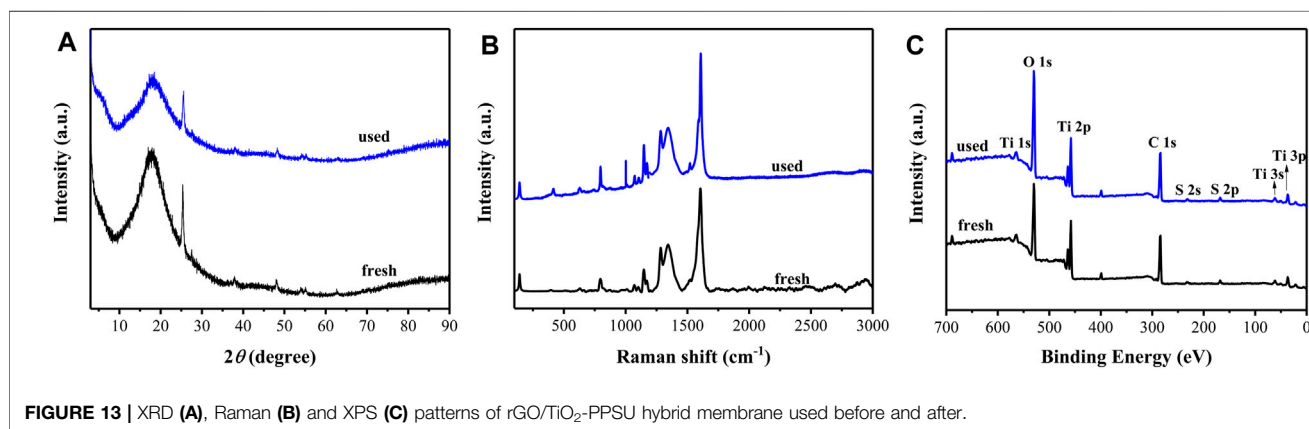


FIGURE 13 | XRD (A), Raman (B) and XPS (C) patterns of rGO/TiO₂-PPSU hybrid membrane used before and after.

removed after water washing and light irradiation. However, there was a sharp decline in R_{ir} and R_t with GO-PPSU, TiO₂-PPSU and rGO/TiO₂-PPSU membranes after UV and visible light irradiation. Among them, the R_{ir} and R_t of rGO/TiO₂-PPSU

membranes were minimum, R_{ir} values 10.06, 6.32 and 5.17%, respectively; R_t values 26.76, 26.75 and 26.72%, respectively. The phenomenon suggested that photocatalytic activity and the photo-induced hydrophilicity of GO/TiO₂-PPSU membranes

under UV and visible light could facilitate the removal of strongly bound PhP and endow the membrane with self-cleaning performance.

The reusability of the rGO/TiO₂-PPSU hybrid membranes was examined at the same experimental conditions. **Figure 12** illustrated that the photodegradation activity of the membranes maintain at 80% degradation rate (decreased about 7%) and the mineralization rate of PhP tended to decreased slightly (5.9%) after operation of eight cycles. To explore the anti-poisoning properties of rGO/TiO₂-PPSU membranes, we carried out XRD, Raman and XPS measurements to observe the phase structure changes before and after operation of eight cycles. There were no obvious variations in XRD (**Figure 13A**) and Raman patterns (**Figure 13B**). In XPS spectra (**Figure 13C**), the intensity of C1s and O1s peaks of used rGO/TiO₂-PPSU membrane was found to be slightly stronger than that of fresh one due to the adsorption of PhP degradation intermediates on it. Taken together, the rGO/TiO₂-PPSU membrane performed well reusability and anti-poisoning properties.

CONCLUSION

In this work, a novel rGO/TiO₂-PPSU hybrid ultrafiltration membrane with enhanced self-cleaning and photodegradation property was fabricated via a non-solvent induced phase-separation method by adding rGO/TiO₂ nanocomposites. The rGO/TiO₂-PPSU composite membrane acquired a higher PhP degradation efficiency than pristine PVDF, GO-PPSU and TiO₂-PPSU membrane under both UV and visible light. Moreover, the rGO/TiO₂-PPSU hybrid ultrafiltration membrane was endowed with a higher permeation flux (348 L/m²h) and water flux recovery rate (>90%) under simulated visible light irradiation due to better self-cleaning performance of the membrane.

REFERENCES

- Abdel-Karim, A., El-Naggar, M. E., Radwan, E. K., Mohamed, I. M., Azaam, M., and Kenawy, E.-R. (2021). High-performance Mixed-Matrix Membranes Enabled by Organically/inorganic Modified Montmorillonite for the Treatment of Hazardous Textile Wastewater. *Chem. Eng. J.* 405, 126964. doi:10.1016/j.cej.2020.126964
- Barzegar, H., Zahed, M. A., and Vatanpour, V. (2020). Antibacterial and Antifouling Properties of Ag₃PO₄/GO Nanocomposite Blended Polyethersulfone Membrane Applied in Dye Separation. *J. Water Process Eng.* 38, 101638. doi:10.1016/j.jwpe.2020.101638
- Brende, B. (2020). *The Global Risks Report*. 15th Edition. Davos, Switzerland: World Economic Forum.
- Chen, Y., Wang, L., Sun, H., Zhang, D., Zhao, Y., and Chen, L. (2021). Self-assembling TiO₂ on Aminated Graphene Based on Adsorption and Catalysis to Treat Organic Dyes. *Appl. Surf. Sci.* 539, 147889. doi:10.1016/j.apsusc.2020.147889
- Dai, J., Li, S., Liu, J., He, J., Li, J., Wang, L., et al. (2019). Fabrication and Characterization of a Defect-free Mixed Matrix Membrane by Facile Mixing PPSU with ZIF-8 Core-Shell Microspheres for Solvent-Resistant Nanofiltration. *J. Membr. Sci.* 589, 117261. doi:10.1016/j.memsci.2019.117261
- Dharupaneedi, S. P., Nataraj, S. K., Nadagouda, M., Reddy, K. R., Shukla, S. S., and Aminabhavi, T. M. (2019). Membrane-based Separation of Potential Emerging Pollutants. *Separat. Purif. Tech.* 210, 850–866. doi:10.1016/j.seppur.2018.09.003
- Ding, S., Sun, S., Xu, H., Yang, B., Liu, Y., Wang, H., et al. (2019). Preparation and Adsorption Property of Graphene Oxide by Using Waste Graphite from diamond Synthesis Industry. *Mater. Chem. Phys.* 221, 47–57. doi:10.1016/j.matchemphys.2018.09.036
- Espíndola, J. C., Cristóvão, R. O., Mendes, A., Boaventura, R. A. R., and Vilar, V. J. P. (2019). Photocatalytic Membrane Reactor Performance towards Oxytetracycline Removal from Synthetic and Real Matrices: Suspended vs Immobilized TiO₂-P25. *Chem. Eng. J.* 378, 122114. doi:10.1016/j.cej.2019.122114
- Gao, Y., Hu, M., and Mi, B. (2014). Membrane Surface Modification with TiO₂-Graphene Oxide for Enhanced Photocatalytic Performance. *J. Membr. Sci.* 455, 349–356. doi:10.1016/j.memsci.2014.01.011
- Georg, Riegel., and James, R. B. (1995). Photocatalytic Efficiency Variability in TiO₂ Particles. *J. Phys. Chem. B.* 99, 4215–4224. doi:10.1021/j100012a050
- Golpour, M., and Pakizeh, M. (2018). Preparation and Characterization of New PA-MOF/PPSU-GO Membrane for the Separation of KHI from Water. *Chem. Eng. J.* 345, 221–232. doi:10.1016/j.cej.2018.03.154
- Hu, F., Sun, S., Xu, H., Li, M., Hao, X., Shao, G., et al. (2021a). Investigation on G-C₃N₄/rGO/TiO₂ Nanocomposite with Enhanced Photocatalytic Degradation Performance. *J. Phys. Chem. Sol.* 156, 110181. doi:10.1016/j.jpcs.2021.110181
- Hu, Y., Zhou, C., Wang, H., Chen, M., Zeng, G., Liu, Z., et al. (2021b). Recent advance of Graphene/semiconductor Composite Nanocatalysts: Synthesis, Mechanism, Applications and Perspectives. *Chem. Eng. J.* 414, 128795. doi:10.1016/j.cej.2021.128795

Moreover, the composite membrane demonstrated an outstanding reusability with a slight drop of photocatalytic efficiency after eight cycles.

DATA AVAILABILITY STATEMENT

The original contributions presented in the study are included in the article/Supplementary Material; further inquiries can be directed to the corresponding authors.

AUTHOR CONTRIBUTIONS

FD: Conceptualization, Methodology, Investigation, Data curation, Writing - original draft, Writing - review and editing, Visualization. SZ: Formal analysis, Investigation, Data curation, Visualization. QW: Investigation, Data curation. HC: Investigation, Visualization. CC: Supervision, Funding acquisition. GQ: Visualization. YY: Methodology, Writing - original draft, Writing - review and editing, Supervision, Funding acquisition.

FUNDING

This work was supported by Research Startup program of Donghua University (285-07-005702).

ACKNOWLEDGMENTS

We thank Lei Liu, Li Wei and Mengyao Zhang for their help in the measurement and characterization of the paper.

- Hummers, W. S., and Offeman, R. E. (1958). Preparation of Graphitic Oxide. *J. Am. Chem. Soc.* 208, 1334–1339. doi:10.1021/ja01539a017
- Hunge, Y. M., Yadav, A. A., Dhodamani, A. G., Suzuki, N., Terashima, C., Fujishima, A., et al. (2020). Enhanced Photocatalytic Performance of Ultrasound Treated GO/TiO₂ Composite for Photocatalytic Degradation of Salicylic Acid under Sunlight Illumination. *Ultrason. Sonochem.* 61, 104849. doi:10.1016/j.ultrsonch.2019.104849
- Iglesias, O., Rivero, M. J., Urriaga, A. M., and Ortiz, I. (2016). Membrane-based Photocatalytic Systems for Process Intensification. *Chem. Eng. J.* 305, 136–148. doi:10.1016/j.cej.2016.01.047
- Kumar, M., Isloor, A. M., Todeti, S. R., Nagaraja, H. S., Ismail, A. F., and Susanti, R. (2021). Effect of Binary Zinc-Magnesium Oxides on Polyphenylsulfone/cellulose Acetate Derivatives Hollow Fiber Membranes for the Decontamination of Arsenic from Drinking Water. *Chem. Eng. J.* 405, 126809. doi:10.1016/j.cej.2020.126809
- Kumari, P., Bahadur, N., and Dumée, L. F. (2020). Photo-catalytic Membrane Reactors for the Remediation of Persistent Organic Pollutants - A Review. *Separat. Purif. Tech.* 230, 115878. doi:10.1016/j.seppur.2019.115878
- Li, N., Chen, G., Zhao, J., Yan, B., Cheng, Z., Meng, L., et al. (2019). Self-cleaning PDA/ZIF-67@PP Membrane for Dye Wastewater Remediation with Peroxymonosulfate and Visible Light Activation. *J. Membr. Sci.* 591, 117341. doi:10.1016/j.memsci.2019.117341
- Liu, S., Jiang, T., Fan, M., Tan, G., Cui, S., and Shen, X. (2021). Nanostructure Rod-like TiO₂-Reduced Graphene Oxide Composite Aerogels for Highly-Efficient Visible-Light Photocatalytic CO₂ Reduction. *J. Alloys Compd.* 861, 158598. doi:10.1016/j.jallcom.2021.158598
- Ma, S., Meng, J., Li, J., Zhang, Y., and Ni, L. (2014). Synthesis of Catalytic Polypropylene Membranes Enabling Visible-Light-Driven Photocatalytic Degradation of Dyes in Water. *J. Membr. Sci.* 453, 221–229. doi:10.1016/j.memsci.2013.11.021
- Meng, M., Li, B., Zhu, Y., Yan, Y., and Feng, Y. (2021). A Novel Mixed Matrix Polysulfone Membrane for Enhanced Ultrafiltration and Photocatalytic Self-Cleaning Performance. *J. Colloid Interf. Sci.* 599, 178–189. doi:10.1016/j.jcis.2021.04.082
- Mohd Hir, Z. A., Abdullah, A. H., Zainal, Z., and Lim, H. N. (2018). Visible Light-Active Hybrid Film Photocatalyst of Polyethersulfone-Reduced TiO₂: Photocatalytic Response and Radical Trapping Investigation. *J. Mater. Sci.* 53, 13264–13279. doi:10.1007/s10853-018-2570-3
- Nguyen, C. H., Tran, M. L., Tran, T. T. V., and Juang, R.-S. (2020). Enhanced Removal of Various Dyes from Aqueous Solutions by UV and Simulated Solar Photocatalysis over TiO₂/ZnO/rGO Composites. *Separat. Purif. Tech.* 232, 115962. doi:10.1016/j.seppur.2019.115962
- Pei, W., Zhang, J., Tong, H., Ding, M., Shi, F., Wang, R., et al. (2021). Removal and Reutilization of Metal Ions on ZIF-67/GO Membrane via Synergistic Photocatalytic-Photothermal Route. *Appl. Catal. B: Environ.* 282, 119575. doi:10.1016/j.apcatb.2020.119575
- Romay, M., Diban, N., Rivero, M. J., Urriaga, A., and Ortiz, I. (2020). Critical Issues and Guidelines to Improve the Performance of Photocatalytic Polymeric Membranes. *Catalysts* 10, 570. doi:10.3390/catal10050570
- Shen, L., Huang, Z., Liu, Y., Li, R., Xu, Y., Jakaj, G., et al. (2020). Polymeric Membranes Incorporated with ZnO Nanoparticles for Membrane Fouling Mitigation: A Brief Review. *Front. Chem.* 8, 224. doi:10.3389/fchem.2020.00224
- Singh, R., Sinha, M. K., and Purkait, M. K. (2020). Stimuli Responsive Mixed Matrix Polysulfone Ultrafiltration Membrane for Humic Acid and Photocatalytic Dye Removal Applications. *Separat. Purif. Tech.* 250, 117247. doi:10.1016/j.seppur.2020.117247
- Tran, D.-T., Mendret, J., Méricq, J.-P., Faur, C., and Brosillon, S. (2020). Study of Permeate Flux Behavior during Photo-Filtration Using Photocatalytic Composite Membranes. *Chem. Eng. Process. - Process Intensification* 148, 107781. doi:10.1016/j.cep.2019.107781
- Wang, Q., Dai, F., Zhang, S., Wang, M., Chen, C., and Yu, Y. (2021). Design of a Novel Poly(aryl Ether Nitrile)-Based Composite Ultrafiltration Membrane with Improved Permeability and Antifouling Performance Using Zwitterionic Modified Nano-Silica. *RSC Adv.* 11, 15231–15244. doi:10.1039/d1ra00376c
- Xu, C., Yang, F., Deng, B., Che, S., Yang, W., Zhang, G., et al. (2021). RGO-wrapped Ti₃C₂/TiO₂ Nanowires as a Highly Efficient Photocatalyst for Simultaneous Reduction of Cr(VI) and Degradation of RhB under Visible Light Irradiation. *J. Alloys Compd.* 874, 159865. doi:10.1016/j.jallcom.2021.159865
- Xu, H., Ding, M., Liu, S., Li, Y., Shen, Z., and Wang, K. (2017). Preparation and Characterization of Novel Polysulfone Hybrid Ultrafiltration Membranes Blended with N-Doped GO/TiO₂ 2 Nanocomposites. *Polymer* 117, 198–207. doi:10.1016/j.polymer.2017.04.022
- Xu, Y., Mo, Y., Tian, J., Wang, P., Yu, H., and Yu, J. (2016). The Synergistic Effect of Graphitic N and Pyrrolic N for the Enhanced Photocatalytic Performance of Nitrogen-Doped graphene/TiO₂ Nanocomposites. *Appl. Catal. B: Environ.* 181, 810–817. doi:10.1016/j.apcatb.2015.08.049
- Yan, X., Huo, L., Ma, C., and Lu, J. (2019). Layer-by-layer Assembly of Graphene Oxide-TiO₂ Membranes for Enhanced Photocatalytic and Self-Cleaning Performance. *Process Saf. Environ. Prot.* 130, 257–264. doi:10.1016/j.psep.2019.08.021
- Yang, K., Yang, Z., Zhang, C., Gu, Y., Wei, J., Li, Z., et al. (2021). Recent Advances in CdS-Based Photocatalysts for CO₂ Photocatalytic Conversion. *Chem. Eng. J.* 418, 129344. doi:10.1016/j.cej.2021.129344
- Zangeneh, H., Zinatizadeh, A. A., Zinadini, S., Feyzi, M., and Bahnemann, D. W. (2019). Preparation and Characterization of a Novel Photocatalytic Self-Cleaning PES Nanofiltration Membrane by Embedding a Visible-Driven Photocatalyst boron Doped-TiO₂SiO₂/CoFe₂O₄ Nanoparticles. *Separat. Purif. Tech.* 209, 764–775. doi:10.1016/j.seppur.2018.09.030
- Zangeneh, H., Zinatizadeh, A. A., and Zinadini, S. (2020). Self-cleaning Properties of L-Histidine Doped TiO₂-CdS/PES Nanocomposite Membrane: Fabrication, Characterization and Performance. *Separat. Purif. Tech.* 240, 116591. doi:10.1016/j.seppur.2020.116591
- Zhang, H., Lv, X., Li, Y., Wang, Y., and Li, J. (2010). P25-graphene Composite as a High Performance Photocatalyst. *ACS Nano* 4, 380–386. doi:10.1021/nn901221k
- Zhang, S., Wang, Q., Dai, F., Gu, Y., Qian, G., Chen, C., et al. (2021). Novel TiO₂ Nanoparticles/Polysulfone Composite Hollow Microspheres for Photocatalytic Degradation. *Polymers* 13, 336. doi:10.3390/polym13030336
- Zhang, W., Ding, L., Luo, J., Jaffrin, M. Y., and Tang, B. (2016). Membrane Fouling in Photocatalytic Membrane Reactors (PMRs) for Water and Wastewater Treatment: A Critical Review. *Chem. Eng. J.* 302, 446–458. doi:10.1016/j.cej.2016.05.071
- Zhou, Z., Shen, Z., Cheng, Z., Zhang, G., Li, M., Li, Y., et al. (2020). Mechanistic Insights for Efficient Inactivation of Antibiotic Resistance Genes: a Synergistic Interfacial Adsorption and Photocatalytic-Oxidation Process. *Sci. Bull.* 65, 2107–2119. doi:10.1016/j.scib.2020.07.015

Conflict of Interest: The authors declare that the research was conducted in the absence of any commercial or financial relationships that could be construed as a potential conflict of interest.

Publisher's Note: All claims expressed in this article are solely those of the authors and do not necessarily represent those of their affiliated organizations, or those of the publisher, the editors and the reviewers. Any product that may be evaluated in this article, or claim that may be made by its manufacturer, is not guaranteed or endorsed by the publisher.

Copyright © 2021 Dai, Zhang, Wang, Chen, Chen, Qian and Yu. This is an open-access article distributed under the terms of the Creative Commons Attribution License (CC BY). The use, distribution or reproduction in other forums is permitted, provided the original author(s) and the copyright owner(s) are credited and that the original publication in this journal is cited, in accordance with accepted academic practice. No use, distribution or reproduction is permitted which does not comply with these terms.